Inorganica Chimica Acta 524 (2021) 120440

Contents lists available at ScienceDirect

Inorganica Chimica Acta

journal homepage: www.elsevier.com/locate/ica

Research paper

2′-Thiophenecarboxaldehyde derived thiosemicarbazone metal complexes of copper(II), palladium(II) and zinc(II) ions: Synthesis, spectroscopic characterization, anticancer activity and DNA binding studies

M. Lavanya [a], J. Haribabu [b,c], K. Ramaiah [d], C. Suresh Yadav [e], Ramesh Kumar Chitumalla [f], Joonkyung Jang [f], R. Karvembu [b], A. Varada Reddy [a,*], M. Jagadeesh [d,*]

[a] Department of Chemistry, Sri Venkateswara University, Tirupati 517502, Andhra Pradesh, India
[b] Department of Chemistry, National Institute of Technology Tiruchirappalli, Tiruchirappalli 620015, Tamil Nadu, India
[c] Facultad de Medicina, Universidad de Atacama, Los Carreras 1579, 1532502 Copiapo, Chile
[d] Department of Chemistry, National Institute of Technology Warangal, Warangal 506004, Telangana, India
[e] Department of Chemistry, Indian Institute of Technology Tirupati, Tirupati 517506, Andhra Pradesh, India
[f] Department of Nanoenergy Engineering, Pusan National University, Busan 46241, Republic of Korea

ARTICLE INFO

Keywords:
Thiophene thiosemicarbazones
Crystal structure analysis
Anticancer activity
DNA binding studies

ABSTRACT

Heterocyclic 5′-methyl-2-thiophenecarboxaldehyde-*N*(4)-un/substituted thiosemicarbazones (**1**–**3**) and their metal complexes with copper(II), palladium(II) and zinc(II) ions (**4**–**11**) were synthesized and characterized by using different spectroscopic techniques like FT-IR, ^{1}H, ^{13}C NMR, UV–Visible and electron paramagnetic spectroscopy, *etc*. The crystal structures of the synthesized thiophene thiosemicarbazone ligands **1**, **2** and **3** were determined unambiguously by single-crystal X-ray diffraction analysis. The EPR spectra of the copper(II) complexes, **4**, **6** and **9** have shown rhombic, normal axial and inverse axial symmetry respectively. Furthermore, the DNA binding study was performed on calf-thymus DNA by absorbance, fluorescence and viscosity measurement methods. Notably, the copper(II) and palladium(II) complexes have strong DNA binding interactions compared to the zinc(II) complexes. The DNA binding constants measured for these complexes were found to be in the range of 1.83×10^{4}–1.45×10^{5} M^{-1}. Further, the newly synthesized complexes were also tested for their *in vitro* anticancer activity against three types of human cancer cell lines (COLO-205, MCF-7 and HepG-2) and one normal cell line (HEK-293). Importantly, the zinc(II) complex (**8**) exhibited potent anticancer activity against HepG-2 with an IC_{50} value of 11.65 ± 1.753 μM compared to the standard drug *cis*-platin. The copper(II) complex, **9** against COLO- 205 with an IC_{50} value of 23.08 ± 1.354 μM, complex **4** against MCF-7 and HepG-2 with IC_{50} values of 39.35 ± 1.825 μM and 35.26 ± 0.354 μM, respectively, and complex **6** against HepG-2 with an IC_{50} value of 38.30 ± 1.385 μM have displayed moderate activity compared to the reference drug *cis*-platin.

1. Introduction

The nitrogen and sulfur functionalized thiosemicarbazone molecules are recognized as the most important biological compounds ever since 2-formylpyridine thiosemicarbazones were found to exert antileukemic activity in mice [1]. Thiosemicarbazones derived from either five- or six-member heterocyclic carbonyl compounds usually adopt anticancer activity. Triapine (3-aminopyridine-2-carboxaldehyde thiosemicarbazones) is one of the best-known examples of highly potent anticancer thiosemicarbazone molecule derived from six-member heterocyclic carbonyl compound [2].

These molecules are identified as one among the best known simple organic ligands designed to coordinate with a variety of transition metal ions *via* thioketo ***S*** and hydrazinic ***N*** atoms, which has an impact in biological applications [3]. In the early 1950 s, Campaigne *et al.* and Behnisch *et al.* reported a number of heterocyclic thiosemicarbazones, among which several thiophene carboxaldehyde-derived thiosemicarbazones exhibited higher activity against the tubercle bacillus [4]. Bavin *et al.* reported some aromatic thiosemicarbazones as potential antituberculosis and antileprosy agents [5]. Some of them, such as thiacetazone [6], have emerged as commercial drugs for dreadful diseases, such as tuberculosis, while some other heterocyclic small

* Corresponding authors.
E-mail addresses: ammireddyv@yahoo.co.in (A. Varada Reddy), jagam@iittp.ac.in (M. Jagadeesh).

https://doi.org/10.1016/j.ica.2021.120440
Received 17 January 2021; Received in revised form 5 April 2021; Accepted 4 May 2021
Available online 6 May 2021
0020-1693/© 2021 Elsevier B.V. All rights reserved.

molecules, such as triapine, are under Phase II clinical trials for cancer chemotherapy [7]. The nature of the heteroaromatic ring and the type of substituents attached to the heterocyclic ring of thiosemicarbazones strongly reflect their biological activities [8].

Therefore, it is clearly understood that the heterocyclic thiosemicarbazones have attracted considerable attention because of their appreciable repeatability, highly beneficial pharmacological properties, and different modes of binding [9]. In addition, most thiosemicarbazones exhibit other biological properties, including antitumor [10-12], antibacterial [13] and antifungal [14-16] activities. Alongside the transition metal complexes of these ligands are also being used for a broad spectrum of medicinal applications towards colon cancer [17,18].

The structural similarity of phenylthiosemicarbazones with phenylthioureas with an additional imine group lying adjacent to the thiourea anion binding site has made them function better pH-switchable anion transporters compared to phenylthioureas [19] and squaramides [20,21]. We also demonstrated that the class of thiosemicarbazone shows the pH switchable transport of anions at pH 4.0 and could be used for the targeted anion efflux from the acidic lysosomal vesicles in the cells [22]. The electroactive thiophene ring on thiosemicarbazone complexes of ruthenium assisted in developing a new biosensor for the determination of glucose [23]. Thus, it is very imperative to design and synthesis of novel thiophene thiosemicarbazones and their metal(II) complex derivatives for their versatile applications in biology, analytical chemistry, and material science.

Herein, we designed and synthesized substituted thiophene thiosemicarbazones and their metal(II) complexes. These complexes were rationally investigated its structural and physicochemical characterizations by using different spectroscopic techniques. Most importantly, the metal complexes are further tested for their *in vitro* anticancer activity against different types of cell lines.

2. Experimental section

2.1. Materials and methods

5′-Methyl-2-thiophenecarboxaldehyde, thiosemicarbazide, 4-methyl-3-thiosemicarbazide, 4-phenyl-3-thiosemicarbazide, copper(II) sulfate, palladium(II) chloride and zinc(II) acetate were purchased from Sigma Aldrich. All the solvents used in this study were obtained from commercial sources and were used without any further purification. The Fourier transform infrared (FT-IR, Nicolet 380) spectra of the compounds were recorded in KBr pellets at room temperature. Experimental absorption studies were carried out using a Shimadzu UV-1800 double beam spectrophotometer. The compounds were confirmed preliminarily by nuclear magnetic resonance spectroscopy (NMR, JEOL resonance 400 MHz NMR spectrometer) at the DST Purse Centre, Sri Venkateswara University, Tirupati. X-ray diffraction (XRD, Bruker APEX 2 X-ray (three-circle)) was used for crystal screening, unit cell determination, and data collection. The X-ray radiation employed was generated from a Mo sealed X-ray tube (K_α = 0.70173 Å with a potential of 40 kV and a current of 40 mA) fitted with a graphite monochromator in parallel mode (175 mm collimator with 0.5 mm pinholes). The data frames were taken at widths of 0.5° 2θ. All non-hydrogen atoms were refined with the anisotropic thermal parameters. The structure was refined (weighted least-squares refinement on F^2) to convergence [24,25]. Olex2 was used for the final data presentation and structure plots [26]. The Electron paramagnetic spectra of copper(II) complexes are recorded by using the Bruker-ER073 instrument as polycrystalline samples.

2.2. Synthesis

The general procedure for the synthesis of 5′-methyl-2-thiophenecarboxaldehyde-*N*(4)-un/substituted thiosemicarbazones (**1**–**3**) is a slight modification of our previous study [27]. The condensation of 5′-methyl-2-thiophenecarboxaldehyde with *N*(4)-un/substituted thiosemicarbazide was performed as follows; an ethanolic solution (15 mL) of equimolar amounts of thiosemicarbazide (10 mmol), 4′-methyl-3-thiosemicarbazide (5 mmol), and 4′-phenyl-3-thiosemicarbazide (5 mmol) was added to an ethanolic (99%) solution of 5′-methyl-2-thiophenecarboxaldehyde (0.01–0.005 mol). Subsequently, 2 mL of acetic acid was added to the reaction mixtures as a catalyst and the entire contents of the flasks were heated under refluxed conditions for about 3 h. The obtained precipitates were filtered, washed with cold ethanol, then purified by recrystallization. The yellow to brown crystalline solids obtained were filtered and dried in a *vacuum*.

2.2.1. 5′-methyl-2-thiophene thiosemicarbazone ($Httsc^1$)/(1)

5′-methyl-2-thiophenecarboxaldehyde (10 mmol, 1.261 g) and thiosemicarbazide (10 mmol, 0.911 g) was added to the ethanolic solution. Subsequently, 2 mL of acetic acid was added during reflux. **Yield:** 1.25 g, (63.1%), Yellow colored solid. M.p: 170–172 °C, Anal. Calc. for $C_7H_9N_3S_2$ (%): C, 42.19; H, 4.55; N, 21.09; S, 32.17, M.Wt: 199.0238; **FT-IR (KBr, υ, cm^{-1}):** 1589 (C═N), 819 (C═S), 1034 (N—N). **UV–Visible (acetonitrile)**: λ_{max}, nm; 250 (π → π), 336 (n → π*). **^{1}H NMR (400 MHz, $CDCl_3$, δ, ppm):** 2.42 (s, 3H, thiophene attached CH_3), 6.42 (s, 1H, thiophene-H), 6.63–6.63 (t, J = 0.8, 1H, thiophene-H), 7.01–7.02 (t, J = 3.2, 2H, NH_2), 7.97 (s, 1H, HC = N), 10.02 (s, 1H, NH). **^{13}C NMR (100 MHz, $CDCl_3$, δ, ppm):** 14.21 (thiophene attached CH_3 carbon), 126.21 (C═N), 131.95, 135.49, 139.00, 144.55 (thiophene carbons), 177.59 (C═S).

2.2.2. 5′-methyl-2-thiophene-N(4)-methylthiosemicarbazone ($Httsc^2$)/(2)

5′-methyl-2-thiophenecarboxaldehyde (5 mmol, 0.630 g) and 4-methyl-3-thiosemicarbazide (5 mmol, 0.525 g), was added to the ethanolic solution. Subsequently 2 mL of acetic acid was added. **Yield:** 1.20 g, (87%), pale brown colored solid, M.p: 240–242 °C, Anal. Calc. for $C_6H_{11}N_3S_2$ (%): C, 45.04; H, 5.20; N, 19.70; S, 30.06. M.Wt: 213.0394; **FT-IR:** 1592 (C═N), 821 (C═S), 1029 (N—N); **UV–Visible (acetonitrile)**: λ_{max}, nm; 245 (π → π), 335 (n → π*). **^{1}H NMR (400 MHz, $CDCl_3$, δ, ppm):** 2.42 (s, 3H, thiophene attached CH_3), 3.16 (d, J = 4.8 Hz, 3H), 6.63–6.64 (d, J = 3.2 Hz, 1H, thiophene-H), 6.98–6.99 (d, J = 3.2 Hz, 1H, thiophene-H), 7.27 (s, 1H, terminal NH), 7.85 (s, 1H, HC = N), 9.67 (s, 1H, NH). **^{13}C NMR (100 MHz, $CDCl_3$, δ, ppm):** 15.79 (thiophene attached CH_3 carbon), 31.6 (terminal CH_3 carbon), 126.14, 131.28, 135.79, 137.39 (thiophene carbons), 143.96 (C═N), 177.79 (C═S).

2.2.3. 5′-methyl-2-thiophene-N(4)-phenylthiosemicarbazone ($Httsc^3$)/(3)

5′-methyl-2-thiophenecarboxaldehyde (5 mmol, 0.630 g) and 4-phenyl-3-thiosemicarbazide (5 mmol, 0.418 g), was added to the ethanolic solution. Subsequently, 2 mL of acetic acid was added. **Yield:** 0.80 g, (80%), Brown colored solid, M.p: 152–154 °C. Anal. Calc. for $C_{13}H_{13}N_3S_2$ (%): C, 56.70; H, 4.76; N, 15.26; S, 23.28. M.Wt: 275.0551; **FT-IR:** 1527 (C═N), 802 (C═S), 1025 (N—N), **UV–Visible (acetonitrile):** λ_{max}, nm; 264 (π → π), 344 (n → π*). **^{1}H NMR (400 MHz, $CDCl_3$, δ, ppm):** 2.48 (s, 3H thiophene attached CH_3 carbon), 6.70–7.08 (m, 2H, thiophene-H), 7.25–7.43 (m, 3H, aromatic-H), 7.64 (d, J = 7.6 Hz, 2H, aromatic-H), 8.11 (s, 1H, C═N), 9.08 (s, 1H, N—H), 11.00 (s, 1H, NH). **^{13}C NMR (100 MHz, $CDCl_3$, δ, ppm):** 15.92 (thiophene attached CH_3 carbon), 124.8, 126.3, 126.3, 128.9 (aromatic), 135.8, 137.9, 138.4, 144.4 (thiophene) 132.0 (C═N), 175.0 (C═S).

2.2.4. Synthesis of metal(II) complexes

2.2.4.1. Bis(5′-methyl-2-thiophenethiosemicarbazonato)(diaqua)copper (II), $[Cu(ttsc^1)_2Cl_2]$/(4). To a hot solution of the free ligand **1** (0.59 mmol, 0.117 g) in ethanol, 10 mL of aqueous $Cu(SO_4)\cdot 5H_2O$ solution (0.18 mol, 0.045 g) was added slowly under stirring. After refluxing for 24 h, the reaction resulted in the formation of a pale yellow colored solution. The progress of the reaction was monitored by TLC using EtOAc:Hexane (7:3) mixture as eluent. A yellow colored solid was

obtained on slow evaporation of the solution. The compound was dried at 100 °C for 2 h and stored in a desiccator. **Yield**: 0.29 g (75%), Brown colored solid, M.p: 225–227 °C. Anal. Calc. for $C_{14}H_{20}CuN_6O_2S_4$ (%): C, 33.89; H, 4.06; N, 16.94; S, 25.85; O, 6.45 Cu, 12.81. M.Wt: 496.1. **FT-IR**: 1557 (C═N), 795 (C═S), 1034 (N—N), 507 (M−S), 441 (M−N). **UV–Visible (ethanol)**: λ_{max}, nm; 235, 269 and 356.

*2.2.4.2. Bis(5′-methyl-2-thiophene thiosemicarbazonato)palladium(II), [Pd(ttsc^1)$_2$]/**(5)**.* To an ethanolic solution of the ligand **1** (2 mmol; 0.426 g), 10 mL of ethanolic solution of $PdCl_2$ (1 mmol; 0.177 g) was added. The reaction mixture was stirred for about 12 h at room temperature. Yellow colored precipitate was obtained and collected by suction filtration and dried in a desiccator over calcium chloride.

Yield: 0.85 g (79%), Brown coloured solid, M.p: 230–232 °C. Anal. Calc. for $C_{14}H_{16}N_6PdS_4$ (%): C, 33.43; H, 3.21; N, 16.71; S, 25.50; Pd, 21.16. M.Wt: 503.0; **FT-IR:** 1579 (C═N), 786 (C═S), 1056 (N—N), 486 (M−S), 430 (M−N). **UV–visible (ethanol)**:λ_{max}, nm; 237, 337 and 401.

*2.2.4.3. Bis(5′-methyl-2-thiophene-N(4)-methylthiosemicarbazonato)(diaqua)copper(II), [Cu(ttsc^2)$_2$Cl$_2$]/**(6)**.* To a hot ethanolic solution of ligand **2** (1.5 mmol, 0.319 g), 10 mL of $Cu(SO_4)_2{\cdot}5H_2O$ solution (0.5 mmol, 0.124 g) was added slowly under stirring. After refluxing for 5 h, the reaction resulted in the formation of a chocolate colored precipitate. The precipitate was then washed with cold ethanol, dried in a hot air oven at 100 °C for 2 h and then stored in a desiccator over anhydrous calcium chloride. **Yield:** 0.88 g (78%), Brown colored solid, M.p: 165–167 °C. Anal. Calc. for $C_{16}H_{24}CuN_6O_2S_4$ (%): C, 36.66; H, 4.62; N, 16.03; S, 24.46; O, 6.10 Cu, 12.12. M.Wt: 524.2. **FT-IR:**1575 (C═N), 798 (C═S), 1047 (N—N), 511 (M−S), 437 (M−N). (703.5); **UV–Visible (ethanol)**: λ_{max}, nm; 234, 380 and 402.

*2.2.4.4. Bis(5′-methyl-2-thiophene-N(4)-methyl-thiosemicarbazonato) palladium(II), [Pd(ttsc^2)$_2$]/**(7)**.* To an ethanolic solution of the ligand **2** (2 mmol, 0.4266 g), 10 mL of ethanolic solution of $PdCl_2$ (1 mmol, 0.177 g) was added. The contents of the round bottom flask were refluxed for about 4 h. The orange coloured precipitate obtained was collected by suction filtration and dried in a hot air oven for about 1 h at 115 °C and then stored in a desiccator over calcium chloride. **Yield:** 0.65 g (79%), Brown coloured solid, M.p: 205–207 °C. Anal. Calc. for $C_{16}H_{20}N_6PdS_4$ (%): C, 36.19; H, 3.80; N, 15.83; S, 24.15; Pd, 20.04. M. Wt: 531.1. **FT-IR:** 1577 (C═N), 800 (C═S), 1047 (N—N), 489 (M−S), 437 (M−N). **UV–visible (ethanol)**: λ_{max}, nm; 231, 239, 285, 350 and 398.

*2.2.4.5. Bis(5′-methyl-2-thiophene-N(4)-methylthiosemicarbazonato) zinc (II), [Zn(ttsc^2)$_2$]/**(8)**.* To an ethanolic solution of the ligand **2** (1.1 mmol, 0.242 g), 10 mL of ethanolic $Zn(OAc)_2{\cdot}2H_2O$ (0.56 mmol, 0.104 g) was added. The reaction mixture was refluxed initially for a period of 2 h and then stirred under room temperature for about 12 h. Pale yellow coloured microcrystals of the complex appeared after stirring. The solid compound was then filtered under suction, washed with cold ethanol and then dried in a hot air oven for about 4 h at 115 °C. **Yield:** 0.40 g (73%), Brown coloured solid, M.p: 235–237 °C. Anal. Calc. for $C_{16}H_{20}N_6S_4Zn$ (%): C, 39.22; H, 4.11; N, 17.15; S, 26.17; Zn, 13.34. M. Wt: 490.0; **FT-IR:** 1581 (C═N), 792 (C═S), 1049 (N—N), 480 (M−S), 439 (M−N). **UV–visible (ethanol)**: λ_{max}, nm; 236, 271 and 357 with a shoulder peak at 374. **^{1}H NMR (400 MHz, CDCl$_3$, δ, ppm):** 2.99–3.00 (d, J = 4.4 Hz, 3H, thiophene attached CH_3), 6.89–6.90 (d, J = 0.4 Hz, 1H), 7.56–7.57 (d, J = 3.2 Hz, 1H, thiophene-H), 7.63–7.64 (d, J = 4.8 Hz, 1H, terminal NH), 7.74 (s, 1H, HC = N). **^{13}C NMR (100 MHz, CDCl$_3$, δ, ppm):** 15.59 (thiophene attached CH_3 carbon), 31.36 (terminal CH_3 carbon), 126.16, 131.93, 134.72, 141.79 (thiophene carbons), 149.12 (C═N), 173.05 (C═S).

*2.2.4.6. Bis(5′-methyl-2-thiophene-N(4)-phenyl-thiosemicarbazonato) (diaqua)copper(II), [Cu(ttsc^3)$_2$(H$_2$O)$_2$]/**(9)**.* To a hot ethanolic solution of ligand **3** (1 mmol, 0.275 g), 10 mL of $Cu(SO_4)_2{\cdot}5H_2O$ (0.33 mmol, 0.083 g) was added slowly under stirring. After refluxing for 5 h, the reaction resulted in the formation of a brown colored precipitate. The precipitate was washed with cold ethanol, dried in a hot air oven at 100 °C for 2 h and then stored in a desiccator over anhydrous calcium chloride. **Yield:** 0.50 g (77%), Brown colored solid, M.p: 152–154 °C. Anal. Calc. For $C_{26}H_{28}CuN_6S_4$ (%): C, 48.17; H, 4.35; N,12.96; S, 19.78; O, 4.94; Cu, 9.80. M.Wt: 648.3. **FT-IR:**1585 (C═N), 792 (C═S), 1058 (N—N), 492 (M−S), 436 (M−N). **UV– Visible (ethanol)**: λ_{max}, nm: 236, 260 and 377.

*2.2.4.7. Bis(5′-methyl-2-thiophene-N(4)-phenylthiosemicarbazonato) palladium(II), [Pd(ttsc^3)$_2$]/**(10)**.* To an ethanolic solution of the ligand **3** (0.91 mmol, 0.252 g), 10 mL of ethanolic solution of $PdCl_2$ (0.45 mmol, 0.081 g) was added. The contents of the round bottom flask were refluxed for about 4 h. Orange coloured precipitate obtained was collected by suction filtration and dried in hot air oven for about 1 h at 115 °C and then stored in a desiccator over calcium chloride. **Yield:** 0.450 g (75%), Orange coloured solid, M.p: 152–154 °C. Anal. Calc. for $C_{26}H_{24}N_6PdS_4$ (%): C, 47.66; H, 3.69; N, 12.83; S, 19.57; Pd, 16.24. M. Wt: 655.2. **FT-IR**:1587 (C═N), 763 (C═S), 1058 (N—N), 493 (M−S), 431 (M−N). **UV–visible (ethanol)**: λ_{max}, nm: 237, 261 and 370.

*2.2.4.8. Bis(5′-methyl-2-thiophene-N(4)-phenyl-thiosemicarbazonato)zinc (II), [Zn(ttsc^3)$_2$]/**(11)**.* To an ethanolic solution of the ligand **3** (0.91 mmol, 0.252 g), 10 mL of ethanolic solution of $Zn(OAc)_2{\cdot}2H_2O$ (0.45 mmol, 0.082 g) was added in solid form and then the reaction mixture was refluxed. After 10 min, the reaction resulted in the formation of a yellow precipitate. Stirring was continued for about 4 h. The precipitate was collected by suction filtration, washed with dry ether and then dried in an oven at 115 °C for about 2 h. **Yield**: 0.42 g (75%), Brown coloured solid, M.p: 152–154 °C. Anal. Calc. for $C_{26}H_{24}N_6S_4Zn$ (%): C, 50.85; H, 3.94; N, 13.68; S, 20.88; Zn, 10.65. M.Wt: 614.1. **FT-IR**: 1596 (C═N), 802 (C═S), 1058 (N—N), 498 (M−S), 476 (M−N).; **UV–Visible (ethanol)** λ_{max}, nm: 241, 260 and 376.

2.3. Computational details

DFT/TDDFT simulations were carried out to explore the structural optical, and electronic properties of the synthesized three 5′-methyl-thiophene-*N*(4)-substituted thiosemicarbazone molecules **1**–**3**. All the reported simulations for the molecules were performed using the Gaussian 09 program [28]. A hybrid Becke, three-parameter, Lee-Yang-Parr functional (B3LYP) in combination with the 6-31G(d) basis set was used for structural relaxation and vibrational frequency analysis [29-31]. Vibrational frequency analysis was carried out to confirm that each configuration is indeed a local minimum on the potential energy surface. The calculated vibrational frequencies were compared with the corresponding experimental values after frequency compensation by a scaling factor of 0.9614, as suggested by Scott and Radom for the B3LYP functional and 6-31G(d) basis set [32].

The ground state optimized geometries of **1**–**3** for single point TDDFT simulations were considered to simulate their UV–visible spectra. In the TDDFT simulations, acetonitrile was used as a solvent to mimic the experimental conditions. The absorption properties in the acetonitrile solvent were calculated using a polarizable continuum model [33,34]. The first 25 singlet–singlet vertical transitions were simulated to calculate the excitation energies and oscillator strengths. All the input files were created and the output files were visualized and analyzed by the GaussView program [35].

2.4. Biological applications

2.4.1. In vitro cytotoxicity

The synthesized complexes of the substituted thiophene thiosemicarbazone ligands were tested for their *in vitro* antiproliferative activity against the tested cancer cell lines such as human colon cancer cell line COLO-205, human breast adenocarcinoma cell line MCF-7, human hepatocellular carcinoma cell line HepG-2 and human embryonic kidney cell line HEK-293. All the cell lines used in this study were obtained from the National Centre for Cell Science (NCCS), Pune, India and are maintained in Dulbecco's Modified Eagle Medium (DMEM) supplemented with 2 mM/L glutamine, 10% fetal bovine serum (FBS) and 10 μg/mL of ciprofloxacin in a 5% CO_2 and 95% air incubator at 37 °C [36-38]. COLO-205, MCF-7, HepG-2 and HEK293 cells were plated into a 96-well plate at a density of 1×10^4 cells/well were seeded in 0.2 mL of DMEM and incubated for 24 h at 37 °C in 5% CO_2 atmosphere. Standard MTT (3-(4,5-dimethylthiazol-2-yl)-2,5-diphenyltetrazolium bromide) assay described previously was employed in this work [39-42].

2.4.2. DNA binding studies

The mode of binding of complexes (**4**–**11**) with the CT-DNA was studied by the electronic absorption and ethidium bromide (EB) fluorescent quenching experiments. The DNA interaction of complexes (**4**–**11**) with CT-DNA was carried out in Tris-HCl/NaCl buffer (pH 7.2). The CT-DNA was dissolved in 50 mM NaCl/5 μM Tris-HCl (pH 7.2) solution. In the UV–vis absorbance spectrum, DNA has shown two peaks at 260 and 280 nm with a 1.9:1 intensity ratio, indicating that the DNA was sufficiently free of proteins. The concentration of CT-DNA was determined from the absorption intensity at 260 nm with the absorption coefficient value of 6600 $M^{-1}cm^{-1}$ [43,44]. Absorption titration experiments were done using different concentrations of CT-DNA while keeping the metal complex concentration constant. Samples were equilibrated before recording each spectrum. The tested metal(II) complexes were 15 μM while the concentration of CT-DNA was changed from 0 to 35 μM. The changes in the absorbance values on each addition of CT-DNA were noted.

The competitive binding of each complex with EB was investigated by fluorescence spectroscopic technique to examine whether the complex can displace the EB from its CT-DNA-EB complex. EB, an intercalating agent to DNA can fluoresce it when bound to polynucleotide molecule 20 times greater than its original fluorescence intensity [45,46]. EB solution was prepared by using Tris-HCl/NaCl buffer (pH 7.2). The test solution was added in aliquots of 5 μM concentration to the DNA-EB complex and the changes in fluorescence intensity at 596 nm (510 nm excitation) was monitored.

2.4.3. Viscosity measurements

Viscosity measurements were carried out using a semi-micro viscometer maintained at 27 °C in a thermostatic water bath. The flow time of solutions in Tris-HCl buffer (pH 7.2) was recorded in triplicate for each sample. An average flow time was calculated from the digital timer attached to the viscometer. For viscosity studies, CT-DNA concentration was kept constant (100 μM) and the concentration of the complexes (**4**–**11**) varied (1/R = [Complex]/[DNA]. Data are presented as η/η^0 *versus* 1/R, where η is the relative viscosity of DNA in the presence of complex (0–60 μM), and$\eta^0$is the relative viscosity of DNA alone. Relative viscosity values were calculated from the observed flow time of the DNA solution (t) corrected for the flow time of the buffer alone (t^0), using the expression $\eta^0 = (t - t^0)/t^0$ [47].

3. Results and discussion

3.1. Computational studies

The theoretical simulations were carried out on **1**, **2,** and **3** to gain insight into their structural, electronic, electrochemical, and photophysical properties. The optimized structures of the molecules are planar (Supplementary data, Fig. S1). Interestingly, the substitution of either methyl (**2**) or phenyl (**3**) on the terminal nitrogen did not disturb the planarity of the molecule significantly.

3.2. Infrared spectra

The infrared spectra of the compounds serve as an important tool for the preliminary confirmation of the synthesized free ligands and their respective metal(II) complexes (**1**–**3** and **4**–**11**, respectively) (see Table S1). The title compounds possess different functional groups, such as the thiophene ring; thiosemicarbazide fragment; and methyl, phenyl, imine, and thione groups. The characteristic vibrations of the compounds observed in the spectra were assigned to the important functional groups in the molecules.

The preliminary confirmation for the formation of the ligands **1**–**3** and thereafter the involvement of azomethine (C═N) group in coordination with the metal(II) ion is strongly established by using FT-IR spectroscopy. The presence of a strong stretching vibration band at 1591, 1593 and 1527 cm^{-1} [48] are assigned to C═N for molecules **1**, **2** and **3**, respectively. The same band has shown a significant shift of about 1 – 32 cm^{-1} towards lower frequency after coordination with the metal (II) ions [49]. The C═S bond vibration is observed at 819, 821, and 802 cm^{-1} for **1**, **2** and **3**, respectively and later after complexation, the same band has shown a considerable shift towards lower frequency after complexation [50,51]. The stretching frequencies for the NH_2 group in compound **1** were observed at 3247 cm^{-1} [52,53]. The structure of the three thiophene appended thiosemicarbazones (**1**–**3**) was determined by ^1H and ^{13}C NMR. In all the three molecules **1**–**3**, the methyl group at the thiophene ring was observed as a singlet at δ: 2.47–2.48 ppm. In compound **2**, the methyl group on the *N*(4) nitrogen was observed as a singlet at δ: 3.22 ppm. After condensation of the thiosemicarbazide, the proton of H–C═N was noted as a singlet at 8.03, 7.98 and 8.11 ppm, respectively, for the three ligands (**1**–**3**) [54]. In compound **1**, the –NH_2 protons are seen as a broad doublet at 7.11 and 6.49 ppm, the substitution of a methyl group at this nitrogen shifted the –N—H(CH_3) proton to 7.33 ppm while in compound **3**, the same N—H proton was shifted to 8.11 ppm. The –N–NH proton was observed at 10.26–11.00 ppm for **1**, **2**, and **3**, respectively. The ^{13}C NMR spectra have shown the C═N and C═S carbons at δ: 144.6 and 177.6 ppm for **1**, at 144.4 and 177.7 ppm for **2** and at 144.4 and 175.0 ppm for **3**. All other protons and carbons were observed in the expected region [55,56].

3.3. UV–Visible spectra

The UV–Visible absorption spectra of ligands (**1**–**3**) and their respective metal(II) complexes were recorded as their ethanolic solutions. The free ligands **(1**–**3)** have shown a similar pattern of absorption spectra. Two different sets of absorption bands are observed for the ligands **1**–**3** between 335 and 345 nm and 200 to 240 nm. The first set of bands are assigned to the n → π* transitions and attributed to the thiosemicarbazone moiety. The absorption maxima in the low-energy region (λ_{max}) of the compounds are noted at 336, 335, and 344 nm for **1**, **2**, and **3**, respectively. Compound **3** has shown a small bathochromic shift in the λ_{max}, when compared with the other two molecules, which could be attributed to the presence of a phenyl ring at the terminal nitrogen atom. The second set of the absorption bands in the far UV region was assigned to the π → π* transitions of the thiophene ring in the molecule [9].

The absorption bands obtained from the TDDFT simulations have resembled those of the experimental data. The most intense absorptions in the low-energy region of **1**, **2**, and **3**were observed at 337, 338, and 355 nm, respectively. As expected, a bathochromic shift of *ca.* 17 nm was observed for **3** compared to **1** and **2**. The simulated UV–Visible absorption spectra have shown an excellent agreement with those obtained from the experimental results. The observed absorption maxima

arise from the HOMO to LUMO transition. Table S2 (Supplementary information) lists out the calculated excitation wavelengths along with their oscillator strengths and coefficient of configuration interaction as well as the dominant contribution to each transition. Both the experimental and simulated spectra are shown for comparison in Fig. 1.

The copper(II) complexes have exhibited the electronic spectra similar to the square planar complexes. Due to close separation between the energy levels, the electronic transitions are not properly resolved. The ground state, d^{22}_{x-y} ($^2B_{1g}$), usually allows three d–d transitions [$^2B_{1g} \rightarrow {}^2E_g$ ($d^{22}_{x-y} \rightarrow d_{xz}, d_{yz}$), $^2B_{1g} \rightarrow {}^2B_{2g}$ ($d^{22}_{x-y} \rightarrow d_{xy}$), $^2B_{1g} \rightarrow {}^2A_{1g}$ ($d^{22}_{x-y} \rightarrow d^2_z$) respectively] which were not seen properly due to the high intense intra-ligand transitions covering the low energy transitions of the metal ion [57-59]. After complexation, the n → π* transitions of the ligand molecules have undergone a considerable red shift to higher wavelength while the π → π* transition has remained almost the same. Another strong band starting at the wavelength 356 nm for **4**, 380 and 402 nm for **6** and at 377 nm for complex **9** tailing into the visible region is understood for the strong metal to ligand charge transfer transition [60].

The usual electronic transitions of the square planar palladium(II)ion are not seen due to overlapping by the intra-ligand charge transfer transitions and metal to ligand charge transfer transitions in the low energy region. The strong absorption band around 400 nm is assignable to a mixture of intra-ligand and ligand to ligand charge transfer [61,62].

The electronic spectra of the tetrahedral zinc(II) complexes [63] is spectra similar to the ligand spectra, which showed the π → π* at 271 and 260 nm, respectively, for the complexes **8** and **11**. Broad and intense bands at around 357 and 376 nm for the complexes slightly extending into the visible region is because of the n → π* transitions overlapped by the ligand to metal charge transfer transitions arising from the S → Zn (II). The spectra without any characteristic absorption band after 500 nm is in good agreement with the d^{10} electronic configuration of zinc(II) ion [64,65]. The absorption spectra of the metal(II) complexes (**4**–**11**) are given in the Supplementary data Fig. S2(a–c).

3.4. HOMO and LUMO energies

The highest occupied molecular orbital (HOMO) and the lowest unoccupied molecular orbital (LUMO) eigenvalues were also calculated for **1**–**3**, as listed in Table 1. Substitution of the methyl group on the *N*(4) nitrogen (i.e., on the transition from **1** to **2**) led to a slight destabilization of the HOMO and LUMO (by *ca.* 0.05 eV), but the HOMO-LUMO gap (HLG) remained almost the same. No shifts in the UV–Visible absorptions can be expected because of the similar HLG for **1** and **2**. In the case of **3** (i.e., on the substitution of phenyl on *N*(4)-nitrogen), although the HOMO is not affected considerably, the LUMO is stabilized by 0.10 eV, which results in a 0.12 eV decrease in the HLG compared to that of **1**. The decreased HLG is responsible for the observed bathochromic shift for the ligand **3**. Table 1 also shows the optical bandgap in eV (i.e., transition energy of $S_0 \rightarrow S_1$) of **1**, **2,** and **3**. The optical bandgap was obtained from the TDDFT calculations. The reported electrochemical bandgaps (*i.e.*, HLG) were *ca.* 0.30 eV smaller than those of the corresponding optical bandgaps.

Table 1
Kohn-Sham eigenvalues of the frontier molecular orbitals, electrochemical (HLG) and optical bandgap ($\mathbf{E_{0\text{-}0}}$) for **1**, **2**, and **3** in acetonitrile.

Compound	HOMO (eV)	LUMO (eV)	HLG (eV)	$E_{0\text{-}0}$(eV)
1	−5.72	−1.74	3.98	3.68
2	−5.67	−1.70	3.97	3.67
3	−5.70	−1.84	3.86	3.49

The isodensity plots and calculated Kohn–Sham eigenvalues of the frontier molecular orbitals of the compounds **1**–**3** with the calculated electrochemical bandgap is shown in Fig. 2. The isodensity plots of the HOMO-1, HOMO, LUMO, and LUMO + 1 of compounds **1**–**3** are shown in Fig. S3 in the Supplementary data. From the electron density distribution, it is evident that the HOMO-1 is localized mainly on the terminal sulfur and three nitrogens. In contrast, the HOMO and LUMO are localized throughout the molecule but in the case of the HOMO, the electron density is slightly more localized on the terminal sulfur atom and in LUMO, the electron density is localized slightly more towards thiophene ring. In the case of LUMO + 1, the electron density is distributed evenly over the entire molecule for **1**, **2,** and **3** (see Fig. S3).

3.5. Molecular electrostatic potential

Molecular electrostatic potential (MEP) maps to assist in understanding the relative polarity of the molecules, sites of electrophilic and nucleophilic reactions, and the hydrogen-bonding interactions. The variation of the colors in the MEP maps specifies the distribution of the electrostatic potential within the molecule. The negative and positive electrostatic potentials are shown in red and blue colors, respectively. The calculated potential grows in the order of red < orange < yellow < green < blue. The simulated MEP plots (Fig. 3) show the negative electrostatic potential (red color) around the thione sulfur atom, which has decreased as the substituent changes from H to CH_3 to Ph. The positive electrostatic potential (blue color) was observed near the imine

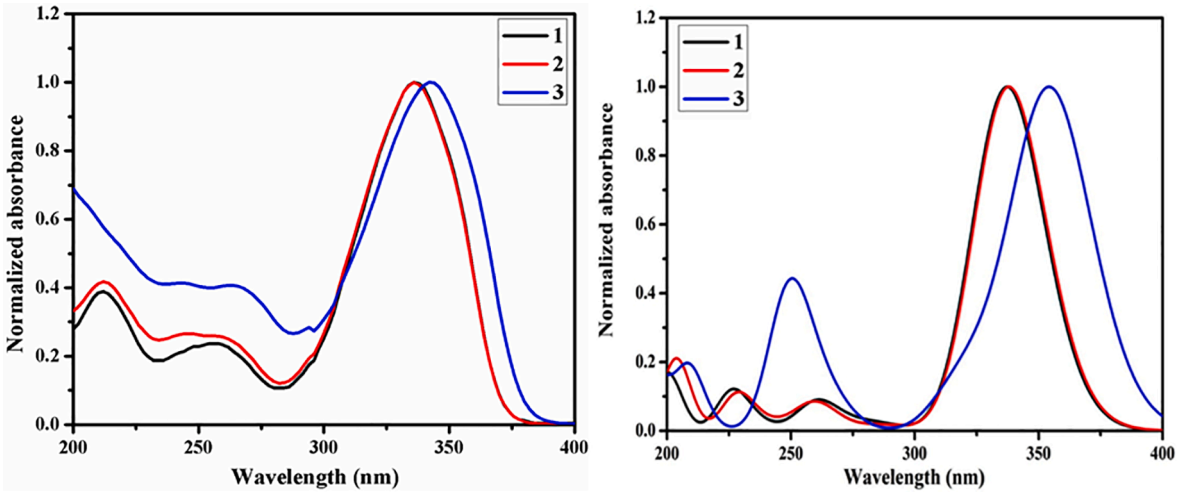

Fig. 1. UV–visible spectra (left) of the thiophene thiosemicarbazones derivatives (**1**–**3**) in comparison with the theoretical spectra (right) obtained from the TDDFT simulations.

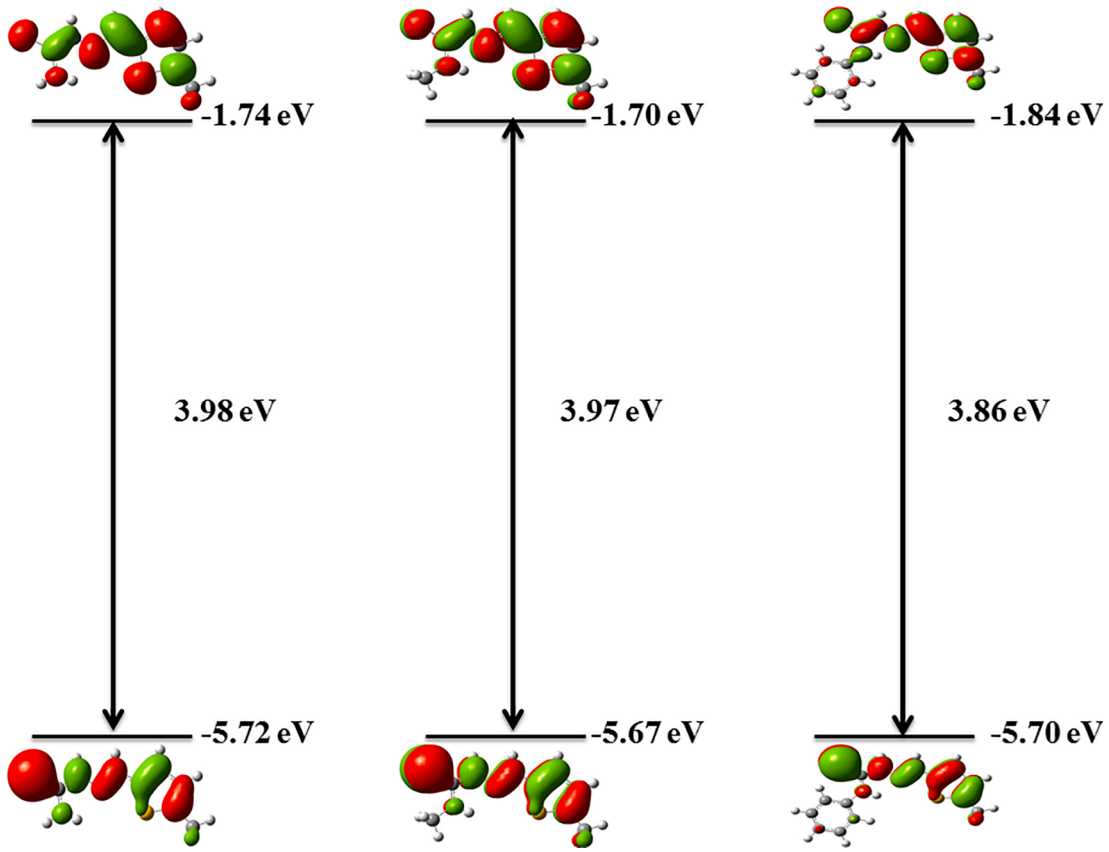

Fig. 2. HOMO-LUMO bandgap for thiophene thiosemicarbazone derivatives (**1**–**3**).

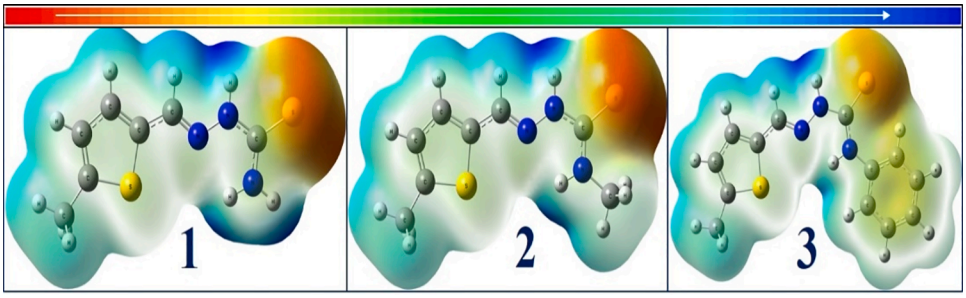

Fig. 3. Molecular Electrostatic Potential (MEP) plot for **1**–**3**. The electrostatic potential increases from red to blue color as shown with an arrow.

group. These sites indicate the atoms that are susceptible to intermolecular hydrogen bonding interactions.

3.6. Density of states

The bandgap of the synthesized molecules, i.e., the separation between the occupied and virtual molecular orbitals can be represented pictorially by the simulated density of states (DOS) and the calculated total DOS for **1**, **2**, and **3** is shown in the supplementary information Fig. S4. The DOS in terms of the Mulliken population analysis was calculated using the GaussSum program. The HOMOs and LUMOs of the molecules are shown as dotted arrows and the corresponding bandgaps (3.98, 3.97, and 3.86 eV for **1**, **2**, and **3**, respectively) are also shown in the same figure. The bandgap was not altered significantly by the substitution of methyl, i.e., in the transition from **1** to **2** but decreased (by 0.12 eV) by the substitution of phenyl, i.e., in the transition from **1** to **3**. The bandgaps shown in the DOS are consistent with the optical bandgaps obtained from TDDFT simulations.

3.7. Single crystal XRD analysis

Single crystal X-ray structural analysis of the ligands revealed that **1** and **3** have crystallized in the triclinic crystal system with the *P*-1 space group. In contrast, the ligand **2** has crystallized in the monoclinic crystal system with the *P*121/*c*1 space group. The crystal structure of each molecule is drawn at 50% probability to show the molecular structure of the compounds (shown in Fig. 4). Table 2 lists the crystal data for the three molecules. The hydrogen-bonding interactions and crystal packing are shown in the Supplementary data Figs. S5a–c.

All three molecules are given an identical numbering scheme to provide an easy way to compare their bond lengths and bond angles. The thiosemicarbazone moiety of these molecules serves as the important part, condensed to a thiophene ring *via* C═N linkage/(C═N–NH–) group and H(**1**)/methyl(**2**)/phenyl(**3**) groups at the nitrogen atom of C(S)NH–. The second position of the thiophene ring is substituted by a 'methyl' group in all three compounds (**1**–**3**). From the crystal data, it is clear that independent molecules (**A** and **B**) were found for compound **1**

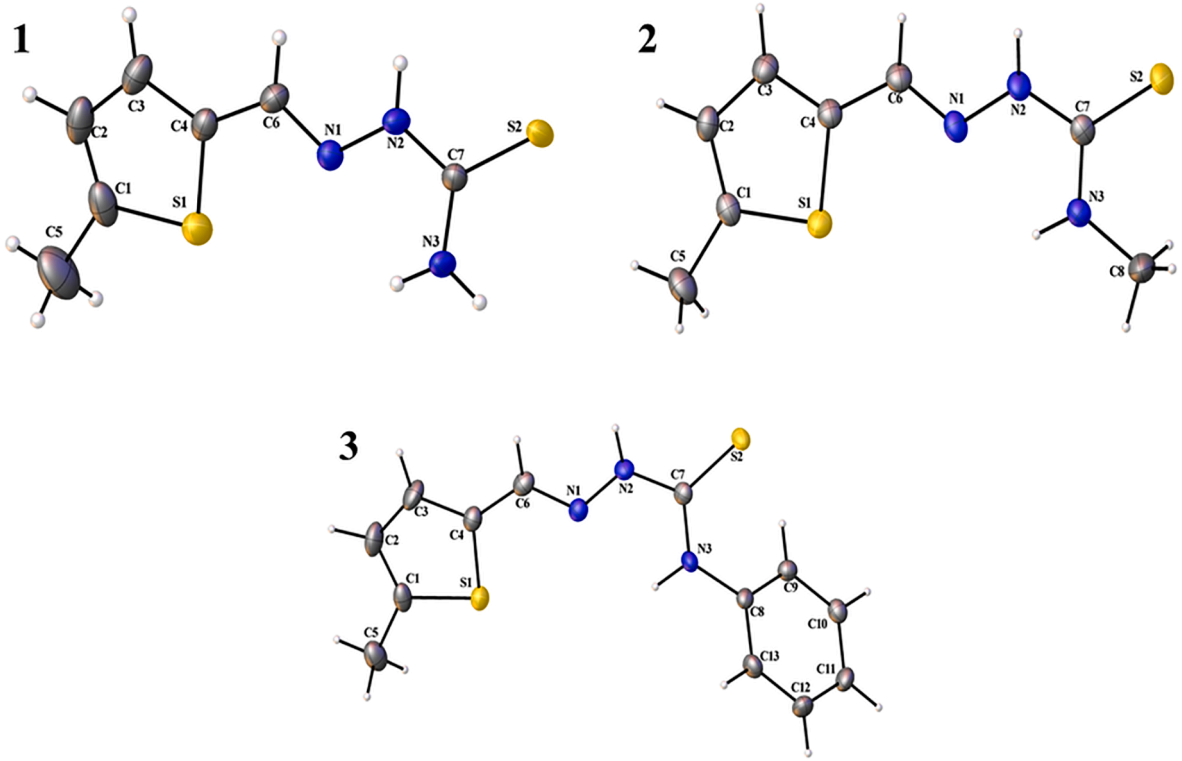

Fig. 4. ORTEP plot for the ligands (**1–3**) drawn at 50% probability.

in the asymmetric unit (see Fig. S6). The torsion angle between the thiophene ring and the thiosemicarbazone part (NNC(S)N) was found to be − 7.86 in **1**, 1.18 in **2** and −0.69 in **3** (giving a slight distortion in planarity of the molecule). In addition, the thiosemicarbazone unit of the compounds (**1–3**) provided solid evidence of the *E*-confirmation around the bond N(2)–C(7). The corresponding bond lengths and bond angles measured for these molecules are in good agreement with each other and were found in the normal ranges (Table S3 lists the selected bond lengths and bond angles of the compounds **1**, **2**, and **3**). The C═S and C═N bond lengths were slightly different from each other, i.e., 1.6958(17) and 1.280(2) Å in **1**, 1.6909(17) and 1.279(2) Å in **2** and 1.681(3) and 1.281(3) Å in **3**, respectively, indicating more a double bond character in compound **3** with respect to the C═S bond and in **2** with respect to the C═N bond. In each molecule, the azomethine group denotes the *trans* to the thione group. Intermolecular hydrogen bonds between N6–H6B…..S2 (D = 3.340 (2) Å, d = 2.5473 Å, θ = 150.30°) can be seen in **1**. Similarly, N—H….S interactions can also be seen in **2** and **3** (For the hydrogen bond distance, see Table S4).

3.8. Electron paramagnetic resonance spectra

The EPR spectra of the Copper(II) complexes have shown two peaks, one with small intensity towards the low field region and the other with large intensity towards the high field region. From the obtained results, the values of $g\|$and$g_\perp$ are calculated which further helps to derive the ground state of the copper ion. The X-band EPR spectra obtained for the three copper(II) complexes of the ligands (**4**, **6** and **9**) at room temperature exhibit well-resolved peaks (Fig. 5) and gives an opportunity to compare the structural environment of the copper ion in the respective complexes. The complex **4** has shown rhombic symmetry with $g_1 > g_2 > g_3$ and $g_1 \neq g_2 \neq g_3$ (g1 = 2.012, g2 = 1.988 and g3 = 1.949) due to low symmetry and the intensity variation depends on the angle θ and φ [66]. The complex, **6**, has adopted normal axial symmetry with $g\| > g_\perp$ (2.0014 and 1.932) while the complex **9** has shown an inverse axial symmetry with $g_\perp > g\|$ (2.114 and 1.888).

3.9. In vitro antiproliferative activity

The *in vitro* antiproliferative activity of the synthesized metal(II) complexes was evaluated by using MTT assay against COLO-205MCF-7 and HepG-2 cell lines. Cis-platin was used as a standard drug and the results are summarized in Table S5 (given in supplementary information). The percentage of cell viability *versus* concentration graphs are shown in Fig. 6. Among all the tested molecules, the two zinc(II) complexes, **8** and **11** have exhibited significant antiproliferative activity against HepG-2 with IC_{50} values of 16.92 ± 1.193 μM and 11.65 ± 1.753 μM, respectively, which are closely comparable with the standard reference compound. The complex **8** has also shown appreciable activity against the COLO-205 (IC_{50}: 12.30 ± 0.164 μM) and MCF-7 (IC_{50}: 21.83 ± 1.369 μM). The copper(II) complex, **9** was found to be moderately active against the COLO- 205 with an IC_{50} value of 23.08 ± 1.354 μM. The remaining complexes have displayed poor activity with IC_{50} values ranging from 28.63 ± 1.36–80.97 ± 0.36 μM. The zinc(II) complexes, **8** and **11** were further tested for their antiproliferative activity against normal cell line HEK-293 (Embryonic Kidney 293) and none of these complexes were found interrupted the viability of the normal cell line, suggesting that the potent compounds are not toxic.

3.10. DNA binding studies

3.10.1. UV–Visible spectroscopic titration

The mode and strength of DNA binding of the synthesized complexes (**4–11**) were studied by UV–visible spectroscopic titration of metal complexes with calf thymus (CT)-DNA [67,68]. To a constant concentration (15 μM) of each of the copper(II), palladium(II) and zinc(II) complexes (**4–11**), eight different concentrations of CT-DNA (0–35 μM) was added slowly. Upon incremental addition of CT DNA to the complexes (**6** and **10**), the absorption intensity decreases, resulting in hypochromism with a small red-shift (see Fig. 7(A)). The DNA binding ability of a compound depends on the extent of wavelength shift and hypochromism and it generally correlates with the intercalative binding

Table 2
Crystal data and structure refinement for **1**–**3**.

Identification code	1	2	3
Empirical formula	$C_7H_9N_3S_2$	$C_8H_{11}N_3S_2$	$C_{13}H_{13}N_3S_2$
Formula weight	199.29	213.32	275.38
Temperature (K)	150.15	150.15	110.15
Wavelength (Å)	0.71073	0.71073	0.71073
Crystal system	Triclinic	Monoclinic	Triclinic
Space group	*P*-1	P 1 21/c1	*P*-1
Unit cell dimensions	a = 5.7851(15); α = 109.094(2) b = 12.783(3); β = 93.810(3) c = 13.688(4); γ = 92.977(2)	a = 7.825(3); α = 90 b = 13.453(5); β = 96.766(4) c = 9.920(4); γ = 90	a = 5.5563; α = 75.351(3) b = 10.622(3); β = 83.177(4) c = 11.642(4); γ = 84.166(4)
Volume ($Å^3$)	951.5(4)	1037.0(7)	685.2(4)
Z, calculated density (Mg m^{-3})	4	4	2
Density (calculated) Mg/m^3	1.391	1.366	1.389
Absorption coefficient (mm^{-1})	0.508	0.471	0.389
F(000)	416	448	288
Crystal size (mm)	0.471 × 0.153 × 0.068	0.54 × 0.53 × 0.21	0.55 × 0.32 × 0.08
Theta range for data collection (°)	1.581 to 27.497	2.563 to 27.579	1.816 to 27.438
Index ranges	$-7 \le h \le 7$, $-16 \le k \le 16$, $-17 \le l \le 17$	$-10 \le h \le 10$, $-17 \le k \le 17$, $-12 \le l \le 12$	$-7 \le h \le 7$, $-13 \le k \le 13$, $-15 \le l \le 15$
Reflections collected/ unique	11,077	11,635	7342
Completeness to theta = 25.242°	99.6%	99.9%	99.4%
Refinement method	Full-matrix least-squares on F^2	Full-matrix least-squares on F^2	Full-matrix least-squares on F^2
Data/restraints/ parameters	4294/0/219	2391/0/120	2943/0/164
Goodness-of-fit on F^2	1.041	1.049	1.134
Final R indices [I > 2σ(I)]	R1 = 0.0319, w*R*2 = 0.0814	R1 = 0.0359, w*R*2 = 0.0911	R1 = 0.0560, w*R*2 = 0.0959
R indices (all data)	R1 = 0.0386, wR2 = 0.0858	R1 = 0.0414, wR2 = 0.0950	R1 = 0.0735, wR2 = 0.1018
Largest diff. peak and hole ($eÅ^{-3}$)	0.357 and −0.273 e.$Å^{-3}$	0.423 and −0.335 e.$Å^{-3}$	0.508 and −0.330 e.$Å^{-3}$
CCDC number reference	1429330	1429331	1429332

efficiency. The observed spectral changes from this study has clearly suggested that the complexes have followed the intercalative mode of binding with the CT-DNA [69]. The binding ability of the complexes and their intrinsic binding constants (K_b) with DNA was calculated by plotting [DNA]/($\varepsilon_a - \varepsilon_f$) against [DNA] according to the equation [DNA]/($\varepsilon_a - \varepsilon_f$) = [DNA]/($\varepsilon_b - \varepsilon_f$) + 1/$K_b$ ($\varepsilon_b - \varepsilon_f$) where [DNA] is the concentration of DNA in base pairs, ε_a is the apparent extinction coefficient value found by calculating A(observed)/[complex], ε_f is the extinction coefficient for the free compound, and ε_b is the extinction coefficient for the compound in the fully bound form. The data obtained for each compound, when fitted into the above equation, gave a straight line with a slope of 1/($\varepsilon_b - \varepsilon_f$) and a y-intercept of 1/K_b ($\varepsilon_b - \varepsilon_f$), and the value of K_b was determined from the ratio of the slope to intercept (Fig. 7 (B)) and intrinsic binding constants (K_b) values are provided in Table 3. The calculated binding constants (K_b) values were found to be in the range of $1.45 \times 10^5 - 1.83 \times 10^4$ M^{-1}. The DNA binding ability of the complexes followed the order **10 > 6 > 4 > 5 > 9 > 7 > 8 > 11**. The above results clearly suggested that palladium(II) [10] and copper(II) [6] complexes penetrate more deeply into and stacks more strongly with

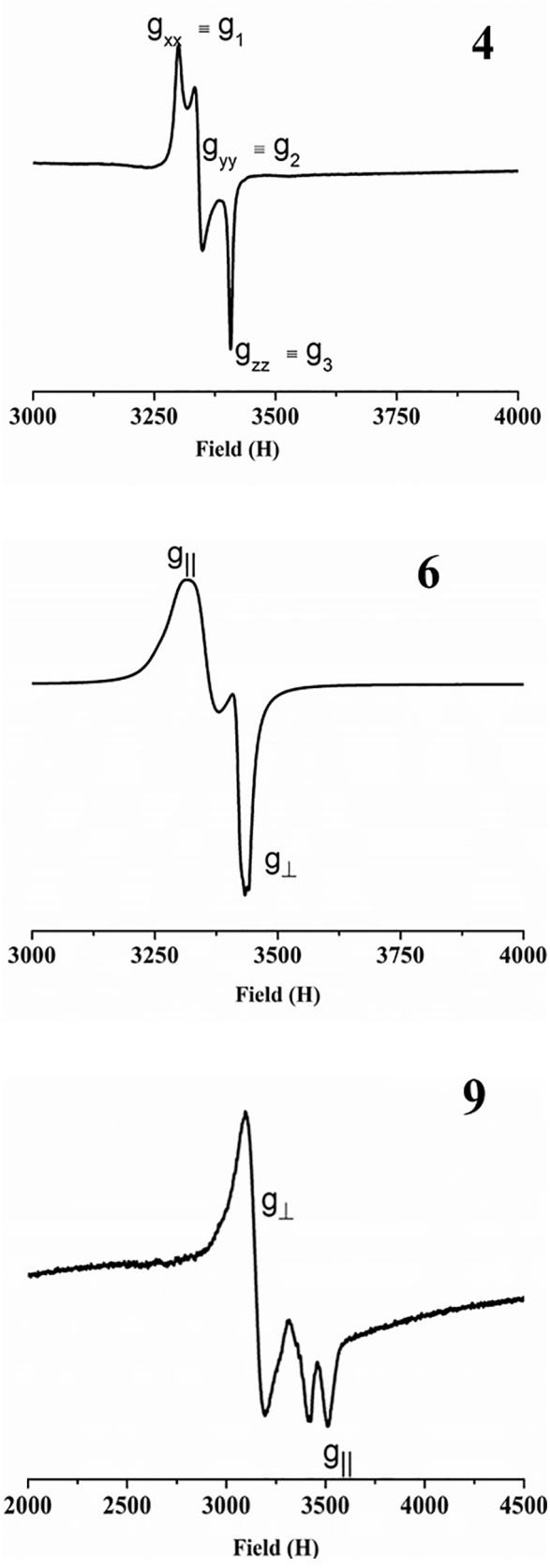

Fig. 5. EPR spectra of polycrystalline copper(II) complexes (**4**, **6** and **9**) recorded at room temperature.

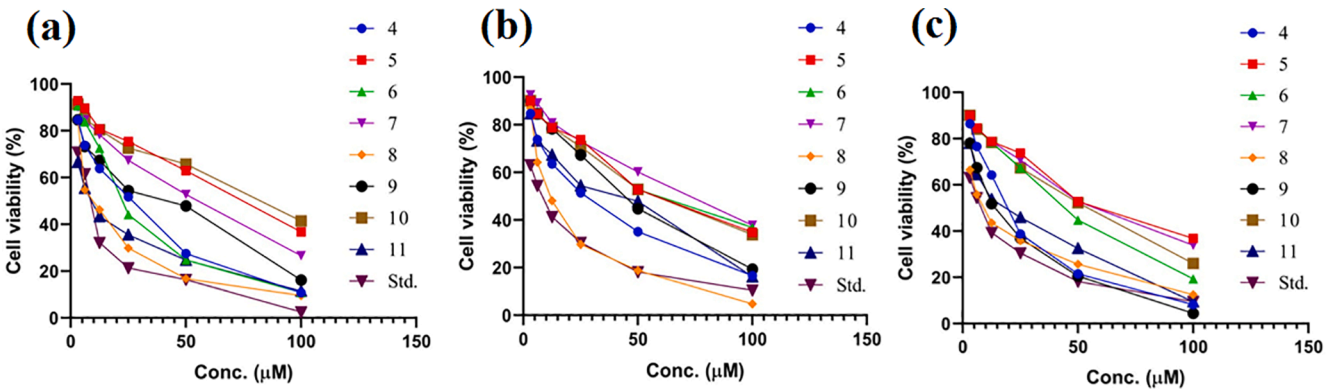

Fig. 6. *In vitro* anticancer activity of the complexes (**4**–**11**) against (a) HepG-2, (b) MCF-7 and (c) COLO-205 cell lines.

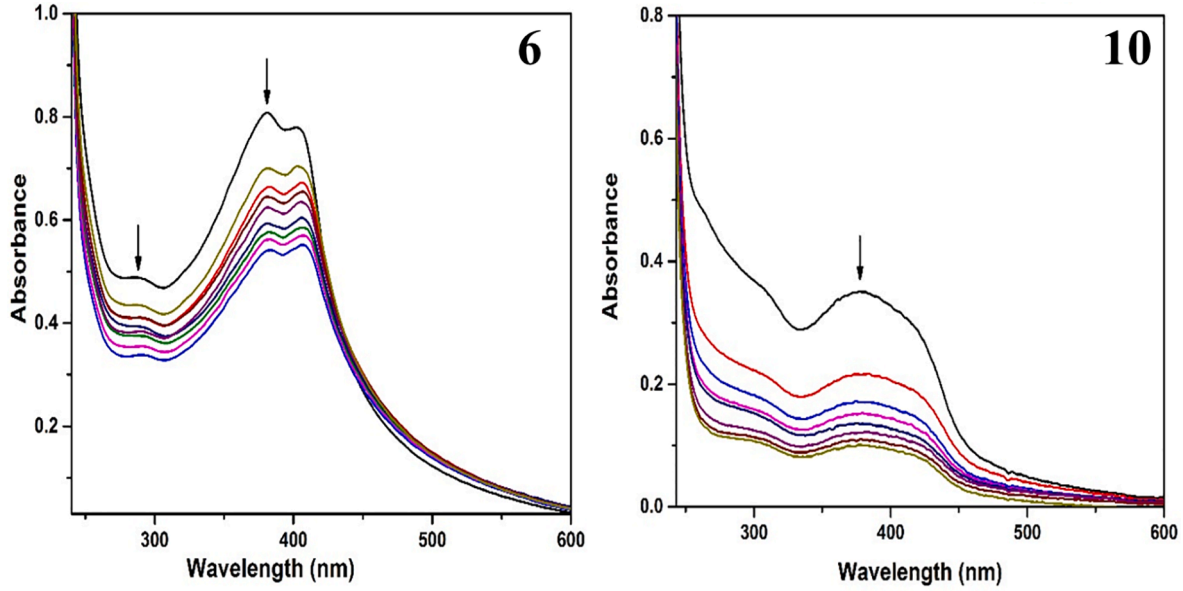

Fig. 7a. Absorption spectra of complexes (**6** and **10**) in Tris-HCl buffer upon addition of CT DNA. [complex] = 15 μM, [DNA] = 0–35 μM. The arrow indicates the decreases in absorption instensity upon increasing the CT DNA concentration.

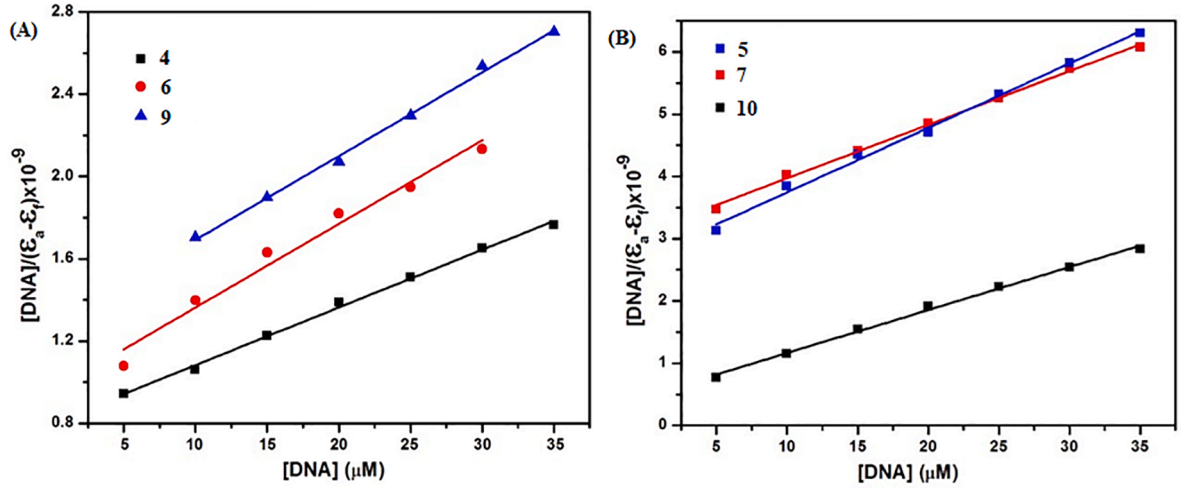

Fig. 7b. Plot of $[DNA]/(\varepsilon_a - \varepsilon_f)$ *versus* [DNA] for the titration of complexes **4–7**, **9** and **10** with CT DNA.

Table 3
DNA binding constant (K_b), Stern-Volmer constant (K_q) and the apparent binding constant (K_{app}) for the complexes.

Complex	K_b (M^{-1})	K_q (M^{-1})	K_{app} (M^{-1})
4	4.24×10^4	3.35×10^4	1.56×10^6
5	3.79×10^4	1.60×10^4	1.00×10^6
6	5.39×10^4	3.19×10^4	1.52×10^6
7	2.73×10^4	1.63×10^4	9.94×10^5
8	2.22×10^4	1.37×10^4	9.20×10^5
9	3.76×10^4	3.93×10^4	1.65×10^6
10	1.45×10^5	1.60×10^4	1.01×10^6
11	1.83×10^4	1.30×10^4	8.94×10^5

base pairs of the CT DNA much effectively than the remaining complexes.

3.10.2. Fluorescence spectroscopic studies

All the complexes (**4**–**11**) are non-emissive in solution at room temperature or in the presence of CT-DNA. So binding of the new complexes with DNA could not be directly predicted *via* the fluorescence spectroscopic technique. Hence, an ethidium bromide (EB) displacement study was carried out to determine the mode of DNA binding with the complexes [70,71]. Ethidium bromide is a typical DNA-intercalator between DNA base pairs through its planar phenanthridine ring resulting in the formation of DNA-EB complex and it emits an intense fluorescence band at 605 nm. Upon gradually increasing the amount of the complexes with CT DNA-EB, there was a decrease in emission intensity of DNA-EB at 605 nm (See Fig. 8). The quenching in the fluorescence intensity indicates that the complexes replaced EB from the DNA-EB complex and bound more strongly with DNA, thus binding of the complexes at the DNA-intercalation sites may be indirectly concluded [11]. The extent of the quenching of DNA-EB reflects the extent of interaction with the added molecule. The quenching of the DNA-EB fluorescence is in good agreement with the liner Stern-Volmerequation [72] $F^o/F = 1 + K_q[Q]$ where F^o and F are the fluorescence intensities in the absence and presence of complex respectively, K_q is a linear Stern-Volmer quenching constant, and [Q] is the concentration of complex. The slope of the plot of F^o/F *versus* [Q] gave K_q (Fig. 8supplementary info). The apparent DNA binding constant (K_{app}) values were calculated by using the equation $K_{EB}[EB] = K_{app}[complex]$ where [complex] is the complex concentration at 50% reduction in the fluorescence intensity of EB, $K_{EB} = 1.0 \times 10^7\ M^{-1}$ and [EB] = 5 μM. The quenching constant $K_q$and K_{app} values are provided in Table 3.

3.11. Viscosity measurements

The binding of the thiophene thiosemicarbazone metal(II) complexes (**4**–**11**) with the calf-thymus (CT) DNA is further determined by the viscosity measurements. Based on the fact that the viscosity of the DNA could change on interaction with the metal complexes or the guest molecules, the binding affinity and mode of binding can be studied through DNA-viscosity measurements. The length of the DNA increases if it adopts a more open structure in order to accommodate the foreign or guest molecule due to its intercalative mode of binding. While the length of the DNA shrinks with the molecules exhibiting covalent interactions, which further bends or kinks the DNA helix. The length of DNA is directly proportional to its viscosity and therefore, the intercalative mode of binding increases the viscosity due to the separation of the DNA base pairs on the addition ofcomplexes. In contrast, the covalent mode of binding decreases the viscosity [73,74]. The changes in the viscosity values of CT DNA (100 μM) in the presence of varying concentration (0–60 μM) of the complexes, **4**–**11** and the resultant data were plotted. Fig. 9 shows that with an increase in the concentration of the complex, the viscosity of DNA system is increasing with subsequent increase in the overall length of DNA [75]. The obtained results clearly suggested that the binding of the complexes with DNA is through the intercalation and the ability of the complexes to increase the viscosity of DNA followed the order **10** > **6** > **4** > **5** > **9** > **7** > **8** > **11**. The zinc(II) complexes (**8** and

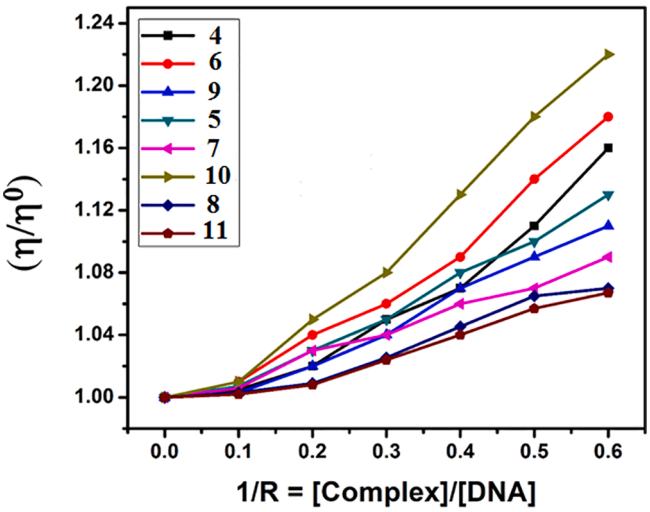

Fig. 9. Viscosity measurements of the complexes showing the effect of increasing concentrations of complexes on the viscosity of CT DNA.

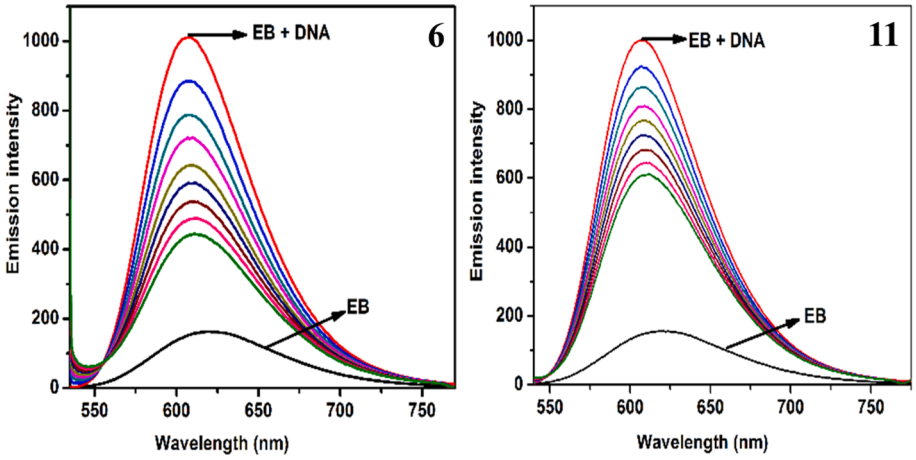

Fig. 8. Fluorescence quenching curves of EB bound to DNA in the presence of **6** and **10** [DNA] = 5 μM, [EB] = 5 μM and [compound] = 0–40 μM.

11) are poor in binding with the CT-DNA whereas the copper(II) (**4**, **6** and **9**) and palladium(II) (**5**, **7** and **10**) complexes of these 5-methyl-*N*(4)-substituted thiosemicarbazone ligands are having a high affinity towards the CT DNA.

4. Conclusion

This paper reported the synthesis and spectroscopic characterization of a set of three bidentate *N*(4)-substituted thiosemicarbazone ligands derived from 5′-methyl-2-thiophenecarboxaldehyde and their complexes of copper(II), palladium(II) and zinc(II) ions. The synthesized compounds were confirmed and characterized using techniques like ^{1}H, ^{13}C NMR, FTIR, and UV–visible, etc. The structural diversity in the substituted thiophene thiosemicarbazones (**1**–**3**) was presented and discussed using the X-ray diffraction studies and DFT calculations. The HOMO-LUMO bandgap for the three ligands was also calculated. This study provides the new avenues for the synthesis of novel copper(II), palladium(II) and zinc(II) complex derivatives for anticancer activities. The zinc(II) complexes, **8** and **11** have shown almost similar antiproliferative activity against HepG2 cell lines when compared with the standard. All the tested metal(II) complexes have shown good interaction with CT-DNA, which was confirmed by spectroscopic and viscosity methods. The motivating results are useful in designing and developing new drugs.

Declaration of Competing Interest

The authors declare that they have no known competing financial interests or personal relationships that could have appeared to influence the work reported in this paper.

Acknowledgments

The author **M. Lavanya** expresses her sincere thanks to **UGC-BSR** for giving fellowship in the RFSMS scheme. The corresponding author, **Dr. M. Jagadeesh**, expresses his gratitude towards **Professor K. N. Satyanarayana**, Director, Indian Institute of Technology Tirupati, Tirupati, for providing research facilities at the institute and for his constant encouragement. A part of this research work was supported by the Korea Research Fellowship program funded by the Ministry of Science, ICT and Future Planning through the National Research Foundation of Korea (2016H1D3A1936765). J. Haribabu express his sincere thanks the Fondo Nacional de Ciencia y Tecnologia (FONDECYT, Project No. 3200391).

Appendix A. Supplementary data

The crystal data were deposited in the CCDC with the numbers 1429330, 1429331 and 1429332. Supplementary data to this article can be found online at https://doi.org/10.1016/j.ica.2021.120440.

References

[1] R.W. Brockman, J.R. Thomson, M.J. Bell, H.E. Skipper, Cancer Res. 16 (1956) 167.
[2] H. Huang, Q. Chen, X. Ku, L. Meng, L. Lin, X. Wang, C. Zhu, Y. Wang, Z. Chen, M. Li, H. Jiang, K. Chen, J. Ding, H. Liu, J. Med. Chem. 53 (2010) 3048.
[3] R. Konakanchi, J. Haribabu, J. Prashanth, N.V. Bharat, M. Ramachary, D. Gandamalla, R. Karvembu, B.V. Reddy, N.R. Yellu, L.R. Kotha, Appl. Organomet. Chem. 32 (2018), e4415.
[4] E. Campaigne, P.A. Monroe, B. Arnwine, W.L. Archer, J. Am. Chem. Soc. 75 (1953) 988.
[5] E.M. Bavin, R.J.W. Rees, J.M. Robson, M. Seiler, D.E. Seymour, D. Suddaby, J. Pharm. Pharmacol. 2 (1950) 764.
[6] D.X. West, H. Beraldo, A.A. Nassar, F.A. El-Saied, M.I. Ayad, Transition Met. Chem. 24 (1999) 595.
[7] A.J. Ocean, P. Christos, J.A. Sparano, D. Matulich, A. Siegel, M. Sung, M.M. Ward, N. Hamel, I. Espinoza-Delgado, Y. Yen, M.E. Lane, Cancer Chemother. Pharmacol. 68 (2011) 379.
[8] C. Balachandran, J. Haribabu, K. Jeyalakshmi, N.S.P. Bhuvanesh, R. Karvembu, N. Emi, S. Awale, J. Inorg. Biochem. 182 (2018) 208.
[9] P.K. Yaman, B. Sen, C.S. Karagoz, E. Subasi, J. Organomet. Chem. 832 (2017) 27.
[10] M. Jagadeesh, S.K. Kalangi, L. Sivarama Krishna, A.V. Reddy, Spectrochim. Acta Part A Mol. Biomol. Spectrosc. 118 (2014) 552.
[11] J. Haribabu, K. Jeyalakshmi, Y. Arun, N.S.P. Bhuvanesh, P.T. Perumal, R. Karvembu, J. Biol. Inorg. Chem. 22 (2017) 461.
[12] C. Shipman, S.H. Smith, J.C. Drach, D.L. Klayman, Antiviral Res. 6 (1986) 197.
[13] R. Ramachandran, M. Rani, S. Kabilan, Bioorg. Med Chem. Lett. 19 (2009) 2819.
[14] K.N. Anees Rahman, K. Ramaiah, G. Rohini, G.P. Stefy, N.S.P. Bhuvanesh, A. Sreekanth, Inorganica Chim. Acta 492 (2018) 131.
[15] R.A. Finch, M.-C. Liu, S.P. Grill, W.C. Rose, R. Loomis, K.M. Vasquez, Y.-C. Cheng, A.C. Sartorelli, Biochem. Pharmacol. 59 (2000) 983.
[16] D. Kovala-Demertzi, J.R. Miller, N. Kourkoumelis, S.K. Hadjikakou, M. A. Demertzis, Polyhedron 18 (1999) 1005.
[17] J.S. Lewis, R. Laforest, T.L. Buettner, S.-K. Song, Y. Fujibayashi, J.M. Connett, M. J. Welch, PNAS 98 (2001) 1206.
[18] G. Munikumari, R. Konakanchi, V.B. Nishtala, G. Ramesh, L.R. Kotha, K. B. Chandrasekhar, C. Ramachandraiah, Synth. Commun. 49 (2019) 146.
[19] N. Busschaert, S.J. Moore, N.J. Wells, J. Herniman, G.J. Langley, P.N. Horton, M. E. Light, I. Marques, P.J. Costa, V. Felix, J.G. Frey, P.A. Gale, Chem. Sci. 4 (2013) 3036.
[20] R.B.P. Elmes, N. Busschaert, D.D. Czeh, P.A. Gale, K.A. Jolliffe, Chem. Commun. 51 (2015) 10107.
[21] N. Busschaert, I.L. Kirby, S. Young, S.J. Coles, P.N. Horton, M.E. Light, P.A. Gale, Angew. Chem. Int. Ed. 51 (2012) 4426.
[22] E.N.W. Howe, N. Busschaert, X. Wu, S.N. Berry, J. Ho, M.E. Light, D.D. Czech, H. A. Klein, J.A. Kitchen, P.A. Gale, J. Am. Chem. Soc. 138 (2016) 8301.
[23] H. Yildirim, E. Guler, M. Yavuz, N. Ozturk, P. KoseYaman, E. Subasi, E. Sahin, S. Timur, Mater. Sci. Eng., C 44 (44) (2014) 1.
[24] G. Sheldrick, Acta Cryst. A 64 (2008) 112.
[25] G. Sheldrick, Acta Cryst. A 71 (2015) 3.
[26] O.V. Dolomanov, L.J. Bourhis, R.J. Gildea, J.A.K. Howard, H. Puschmann, J. Appl. Crystallogr. 42 (2009) 339.
[27] M. Jagadeesh, H.K. Rashmi, Y. Subba Rao, A. Sreenath Reddy, B. Prathima, P. Uma Maheswari Devi, A.V. Reddy, Spectrochim. Acta Part A Mol. Biomol. Spectrosc. 115 (2013) 583.
[28] M. J. Frisch, G. W. Trucks, H. B. Schlegel, G. E. Scuseria, M. A. Robb, J. R. Cheeseman, G. Scalmani, V. Barone, B. Mennucci, G. A. Petersson, H. Nakatsuji, M. Caricato, X. Li, H. P. Hratchian, A. F. Izmaylov, J. Bloino, G. Zheng, J. L. Sonnenberg, M. Hada, M. Ehara, K. Toyota, R. Fukuda, J. Hasegawa, M. Ishida, T. Nakajima, Y. Honda, O. Kitao, H. Nakai, T. Vreven, J. A. Montgomery, J. E. Peralta, F. Ogliaro, M. Bearpark, J. J. Heyd, E. Brothers, K. N. Kudin, V. N. Staroverov, R. Kobayashi, J. Normand, K. Raghavachari, A. Rendell, J. C. Burant, S. S. Iyengar, J. Tomasi, M. Cossi, N. Rega, J. M. Millam, M. Klene, J. E. Knox, J. B. Cross, V. Bakken, C. Adamo, J. Jaramillo, R. Gomperts, R. E. Stratmann, O. Yazyev, A. J. Austin, R. Cammi, C. Pomelli, J. W. Ochterski, R. L. Martin, K. Morokuma, V. G. Zakrzewski, G. A. Voth, P. Salvador, J. J. Dannenberg, S. Dapprich, A. D. Daniels, Farkas, J. B. Foresman, J. V. Ortiz, J. Cioslowski, D. J. Fox, Gaussian 09, Revision B.01, in, Wallingford CT, (2009).
[29] A.D. Becke, J. Chem. Phys. 98 (1993) 5648.
[30] A.D. Becke, J. Chem. Phys. 104 (1996) 1040.
[31] C. Lee, W. Yang, R.G. Parr, Phys. Rev. B 37 (1988) 785.
[32] A.P. Scott, L. Radom, J. Phys. Chem. 100 (1996) 16502.
[33] S. Miertuš, E. Scrocco, J. Tomasi, Chem. Phys. 55 (1981) 117.
[34] M. Cossi, V. Barone, R. Cammi, J. Tomasi, Chem. Phys. Lett. 255 (1996) 327.
[35] R. Dennington, T. Keith, J. Millam, K. Eppinnett, W. L. Hovell and R. Gilliland, GaussView, Version 4.1, Semichem, Inc., Shawnee Mission, KS, 2003.
[36] A. Navya, H. Rashmi, Hari Prasad, P. Uma Maheswari Devi, Int. J. Adv. Pharm. Res. 4 (2013) 2222.
[37] R. Mallela, R. Konakanchi, R. Guda, N. Munirathinam, D. Gandamalla, N.R. Yellu, L.R. Kotha, Inorganica Chim. Acta 469 (2018) 66.
[38] K. Ramaiah, K. Srishailam, K. Laxma Reddy, B.V. Reddy, G. Ramana Rao, J. Mol. Struct. 1184 (2019) 405.
[39] M. Jagadeesh, H.K. Rashmi, Y. Subba Rao, A. Sreenath Reddy, B. Prathima, P. Uma Maheswari Devi, A. Varada Reddy, Spectrochim. Acta Part A Mol. Biomol. Spectrosc. 115 (2013) 583.
[40] R. Konakanchi, R. Mallela, R. Guda, L.R. Kotha, Res. Chem. Intermed. 44 (2018) 27.
[41] Y.C. Huang, J. Haribabu, C.M. Chien, G. Sabapathi, C.K. Chou, R. Karvembu, P. Venuvanalingam, W.M. Ching, M.L. Tsai, S.C.N. Hsu, J. Inorg. Biochem. 194 (2019) 74.
[42] J. Haribabu, S. Srividya, R. Umapathi, D. Gayathri, P. Venkatesu, N. Bhuvanesh, R. Karvembu, Inorg. Chem. Commu. 119 (2020), 108054.
[43] N. Balakrishnan, J. Haribabu, A.K. Dhanabalan, S. Swaminathan, S. Sun, D. F. Dibwe, N. Bhuvanesh, S. Awale, R. Karvembu, Dalton Trans. 49 (2020) 9411.
[44] K. Jeyalakshmi, J. Haribabu, N.S.P. Bhuvanesh, R. Karvembu, Dalton Trans. 45 (2016) 12518.
[45] J. Haribabu, C. Balachandran, M.M. Tamizh, Y. Arun, N.S.P. Bhuvanesh, S. Aoki, R. Karvembu, J. Inorg. Biochem. 205 (2020), 110988.
[46] J. Haribabu, K. Jeyalakshmi, Y. Arun, N.S.P. Bhuvanesh, P.T. Perumal, R. Karvembu, RSC Adv. 5 (2015) 46031.
[47] J. Haribabu, G. Sabapathi, M.M. Tamizh, C. Balachandran, N.S.P. Bhuvanesh, P. Venuvanalingam, R. Karvembu, Organometallics 37 (2018) 1242.
[48] C. Ravikumar, I.H. Joe, V.S. Jayakumar, Chem. Phys. Lett. 460 (2008) 552.
[49] B. Singh, H.J. Mishra, Ind. Chem. Soc. 63 (1986) 692.
[50] B. Sen, H.K. Kalhan, V. Demir, E.E. Guler, H.A. Kayali, E. Subasi, Mater. Sci. Eng., C 98 (2019) 550.

[51] D.X. West, I.S. Billeh, J.P. Jasinski, J.M. Jasinski, R.J. Butcher, Transition Met. Chem. 23 (1998) 209.
[52] K. Ramaiah, J. Prashanth, J. Haribabu, K.E. Sreekanth, B.V. Reddy, R. Karvembu, K. Laxma Reddy, J. Mol. Struct. 1175 (2019) 769.
[53] G.M. de Lima, J.L. Neto, H. Beraldo, H.G.L. Siebald, D.J. Duncalf, J. Mol. Struct. 604 (2002) 287.
[54] S. Saranya, J. Haribabu, V.N.V. Palakkeezhillam, P. Jerome, K. Gomathi, K. Kameswara Rao, V.H.H. Surendra Babu, R. Karvembu, D. Gayathri, J. Mol. Struct. 1198 (2019), 126904.
[55] A.A. Ali, H. Nimir, C. Aktas, V. Huch, U. Rauch, K.H. Schafer, M. Veith, Organometallics 31 (2012) 2256.
[56] J.F. de Oliveira, A.L. da Silva, D.B. Vendramini-Costa, C.A. de Cruz Amorim, J. F. Campos, A.G. Ribeiro, R.O. de Moura, J.L. Neves, A.L.T. Gois Ruiz, J.E. de Carvalho, M.C.A. de Lima, J. Med. Chem. 104 (2015) 148.
[57] M. Muralisankar, S. Sujith, N.S.P. Bhuvanesh, A. Sreekanth, Polyhedron 118 (2016) 103.
[58] P. Naveen, R. Jain, P. Kalaivani, R. Shankar, F. Dallemer, R. Prabhakaran, New J. Chem. 41 (2017) 8885.
[59] A.B.P. Lever, Inorganic Electronic spectroscopy, 33, Elsevier, 1984.
[60] K.N. Anees Rahman, J. Haribabu, C. Balachandran, N.S.P. Bhuvanesh, R. Karvembu, A. Sreekanth, Polyhedron 135 (2017) 26.
[61] P. Paul, S. Bhattacharya, J. Chem. Sci. 126 (2014) 1547.
[62] J. Haribabu, S. Srividya, D. Mahendriran, D. Gayathri, V. Venkatramu, N. Bhuvanesh, R. Karvembu, Inorg. Chem. 59 (2020) 17109.
[63] J. Haribabu, S. Priyarega, N.S.P. Bhuvanesh, R. Karvembu, J. Struct. Chem. 61 (2020) 66.
[64] N. Balakrishna, J. Haribabu, D. Anantha Krishna, S. Swaminathan, D. Mahendiran, N.S.P. Bhuvanesh, R. Karvembu, Polyhedron 170 (2019) 188.
[65] A. Sreekanth, S. Sivakumar, M.R.P. Kurup, J. Mol. Struct. 655 (2003) 47.
[66] K.E. Prosser, C.J. Walsby, Eur. J. Inorg. Chem. 12 (2017) 1573.
[67] A. Shanmugapriya, R. Jain, D. Sabarinathan, G. Kalaiarasi, F. Dallemer, R. Prabhakaran, New J. Chem. 41 (2017) 10324.
[68] K. Jeyalakshmi, J. Haribabu, C. Balachandran, N.S.P. Bhuvanesh, N. Emi, R. Karvembu, New J. Chem. 41 (2017) 2672.
[69] J. Haribabu, G. Sabapathi, M.M. Tamizh, C. Balachandran, N.S.P. Bhuvanesh, P. Venuvanalingam, R. Karvembu, Organometallics 37 (2018) 1242.
[70] J.R. Lakowicz, G. Webber, Biochemistry 12 (1973) 4161–4170, New J. Chem. 42 (2018) 10818.
[71] K. Jeyalakshmi, J. Haribabu, C. Balachandran, E. Narmatha, N.S.P. Bhuvanesh, S. Aoki, R. Karvembu, New J. Chem. 43 (2019) 3188.
[72] K.S. Ghosh, B.K. Sahoo, D. Jana, S. Dasgupta, J. Inorg. Biochem. 102 (2008) 1711.
[73] A. Tadic, J. Poljarevic, M. Krstic, M. Kajzerberger, S. Arandelovic, S. Radulovic, C. Kakoulidou, A.N. Papadopoulos, G. Psomas, S. Grguric-Sipka, New J. Chem. 42 (2018) 3001.
[74] N. Chitrapriya, V. Mahalingam, M. Zeller, K. Natarajan, Inorg. Chem. Acta. 363 (2010) 3685.
[75] E. Gao, J. Xing, Y. Qu, X. Qiu, M. Zhu, Appl. Organometal. Chem. 32 (2018), e4469.